Conformational propensities of intrinsically disordered proteins influence the mechanism of binding and folding

Munehito Arai[a,b,c], Kenji Sugase[a,1], H. Jane Dyson[a], and Peter E. Wright[a,2]

[a]Department of Integrative Structural and Computational Biology and Skaggs Institute for Chemical Biology, The Scripps Research Institute, La Jolla, CA 92037; [b]Department of Life Sciences, Graduate School of Arts and Sciences, The University of Tokyo, Meguro, Tokyo 153-8902, Japan; and [c]Precursory Research for Embryonic Science and Technology, Japan Science and Technology Agency, Kawaguchi, Saitama 332-0012, Japan

Contributed by Peter E. Wright, June 29, 2015 (sent for review May 21, 2015; reviewed by Martin Blackledge and David Eliezer)

Intrinsically disordered proteins (IDPs) frequently function in protein interaction networks that regulate crucial cellular signaling pathways. Many IDPs undergo transitions from disordered conformational ensembles to folded structures upon binding to their cellular targets. Several possible binding mechanisms for coupled folding and binding have been identified: folding of the IDP after association with the target ("induced fit"), or binding of a prefolded state in the conformational ensemble of the IDP to the target protein ("conformational selection"), or some combination of these two extremes. The interaction of the intrinsically disordered phosphorylated kinase-inducible domain (pKID) of the cAMP-response element binding (CREB) protein with the KIX domain of a general transcriptional coactivator CREB-binding protein (CBP) provides an example of the induced-fit mechanism. Here we show by NMR relaxation dispersion experiments that a different intrinsically disordered ligand, the transactivation domain of the transcription factor c-Myb, interacts with KIX at the same site as pKID but via a different binding mechanism that involves elements of conformational selection and induced fit. In contrast to pKID, the c-Myb activation domain has a strong propensity for spontaneous helix formation in its N-terminal region, which binds to KIX in a predominantly folded conformation. The C-terminal region of c-Myb exhibits a much smaller helical propensity and likely folds via an induced-fit process after binding to KIX. We propose that the intrinsic secondary structure propensities of pKID and c-Myb determine their binding mechanisms, consistent with their functions as inducible and constitutive transcriptional activators.

intrinsically disordered protein | coupled folding and binding | NMR relaxation | transcriptional coactivator CBP | transcriptional activator c-Myb

Intrinsically disordered proteins (IDPs) are abundant in eukaryotes and are involved in critical cellular functions, including transcription, translation, and cell cycle control (1–4). Many IDPs fold upon binding to their cellular targets (5) and an understanding of the mechanism of coupled folding and binding is essential for understanding how they perform their biological functions. One of the best studied IDPs is the phosphorylated kinase-inducible domain (pKID) of the cAMP-response element binding (CREB) protein, which interacts with the KIX domain of the transcriptional coactivator CREB-binding protein (CBP) (6). CREB is an inducible transcriptional activator, and phosphorylation of the KID domain at S133 is critical for binding to KIX and for target gene expression (7, 8). The αB helix of unbound pKID is unstructured (9), but folds into helical structure upon binding to KIX (6). NMR relaxation dispersion experiments showed that coupled folding and binding occur by an induced-fit mechanism, in which pKID first forms encounter complexes with KIX, then forms a partly folded intermediate, and finally folds into the fully bound state without dissociation from KIX (10).

CBP is a general transcriptional coactivator that possesses acetyltransferase activity and mediates interactions between transcription factors and the basal transcription machinery (11). The KIX domain of CBP can bind the intrinsically disordered transactivation domains (TADs) of numerous transcription factors, including CREB, c-Myb, and the mixed-lineage leukemia (MLL) protein (4). The TADs of CREB (pKID) and c-Myb bind to a hydrophobic groove formed by the first and third α-helices of KIX (6, 8, 12, 13), whereas the TAD of MLL binds to a different surface, at the interface between the G_2 3_{10}-helix and the second and third α-helices of KIX (12, 14). The proto-oncogene c-Myb is a constitutive transcriptional activator that regulates proliferation and differentiation of hematopoietic cells, whose aberrant amplification has been observed in leukemia (15). The TAD of c-Myb is only partly structured in the free form and can be categorized as an IDP (8). Unlike pKID, which binds tightly to KIX only after phosphorylation at S133, c-Myb interacts with KIX independent of posttranslational modifications (8, 16). Although pKID and c-Myb bind as amphipathic helices to the same site on KIX, there is no obvious sequence similarity between them (6, 8, 13). Thus, pKID and c-Myb constitute a good model system for elucidating the determinants of coupled folding and binding mechanisms.

The present work addresses the mechanism of coupled folding and binding of c-Myb to KIX, using NMR R_2 relaxation dispersion experiments, where R_2 is the transverse relaxation rate.

Significance

Intrinsically disordered proteins play a central role in cellular signaling and regulatory networks. Many regulatory proteins contain disordered recognition motifs that fold upon binding to their cellular targets, by mechanisms that are poorly understood. Here we show that the disordered transactivation domain of the transcription factor c-Myb binds to the KIX domain of the transcriptional coactivator cAMP-response element binding (CREB-binding) protein (CBP) by a mechanism that involves elements of conformational selection and induced fit. In contrast, the phosphorylated kinase-inducible activation domain of CREB binds to the same site on KIX by an induced-fit mechanism. The intrinsic secondary structure propensities of these two disordered proteins determine their binding mechanisms, consistent with their functions as inducible and constitutive transcriptional activators.

Author contributions: M.A., H.J.D., and P.E.W. designed research; M.A. and K.S. performed research; M.A., K.S., H.J.D., and P.E.W. analyzed data; and M.A., K.S., H.J.D., and P.E.W. wrote the paper.

Reviewers: M.B., Institut de Biologie Structurale; and D.E., Weill Cornell Medical College.

The authors declare no conflict of interest.

[1]Present address: Department of Molecular Engineering, Graduate School of Engineering, Kyoto University, Katsura, Nishikyo-ku, Kyoto 615-8510, Japan.

[2]To whom correspondence should be addressed. Email: wright@scripps.edu.

This article contains supporting information online at www.pnas.org/lookup/suppl/doi:10.1073/pnas.1512799112/-/DCSupplemental.

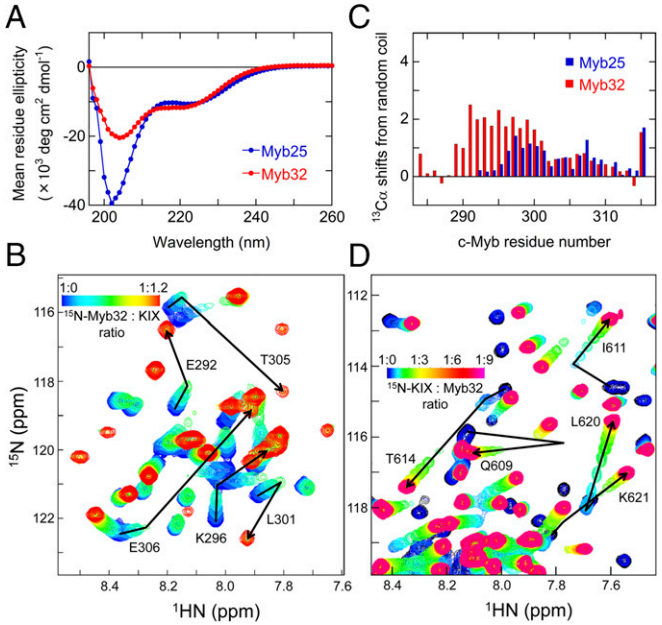

Fig. 1. Conformational propensities of free c-Myb. (*A*) Far-UV CD spectra of free Myb32 (red) and Myb25 (blue). (*B*) Portion of a series of ^{1}H-^{15}N HSQC spectra of ^{15}N-labeled Myb32 showing chemical shift changes upon titration with KIX. The cross-peak color changes gradually from blue (free) to red (bound) according to the concentration ratios shown. The complete spectrum is shown in Fig. S1. (*C*) Secondary $^{13}C_{\alpha}$ chemical shifts of free Myb32 (red) and Myb25 (blue). (*D*) Portion of a series of ^{1}H-^{15}N HSQC spectra of ^{15}N-labeled KIX showing chemical shift changes upon titration with Myb32. The cross-peak color changes gradually from black (free) to magenta (bound) according to the concentration ratios shown. The complete spectrum is shown in Fig. S1.

This powerful technique provides information on protein dynamics in the microsecond to millisecond time range (17) and can provide atomic resolution insights into coupled folding and binding processes of IDPs (10, 18). We found that, unlike pKID, c-Myb binds KIX in a two-state manner without formation of observable intermediates and that the association kinetics strongly depend on the residual helical structure present in the N-terminal portion of c-Myb. The binding mechanisms of these two disordered domains therefore differ, even though they bind to the same site on KIX.

Results

Helix-Forming Propensity of Free c-Myb. The c-Myb TAD used in this work (residues 284–315, termed Myb32) is longer than used in previous studies (residues 291–315; Myb25) (8, 13, 14) and binds more tightly to KIX (see below). Far-UV circular dichroism (CD) spectra show that free Myb32 and Myb25 are mostly unstructured, although Myb32 shows a greater propensity for helix than Myb25 (Fig. 1*A*). The ^{1}H-^{15}N heteronuclear single quantum coherence (HSQC) spectrum of free Myb32 shows little dispersion in the ^{1}H dimension, confirming that Myb32 is disordered in the free form (Fig. 1*B* and Fig. S1*A*, blue peaks).

Secondary $^{13}C_{\alpha}$ chemical shifts of free Myb32, calculated by subtraction of sequence-corrected random coil shifts (19, 20), are shown in Fig. 1*C* together with data for Myb25 (8). The $^{13}C_{\alpha}$ shifts indicate that the central regions of both constructs are partially helical and show that the additional residues at the N terminus of Myb32 extend and stabilize the helical structure. Using the parameterization of Yao et al. (21), the population of helix in the region between residues 290 and 301 of Myb32 was estimated to be ~70% from sequence-corrected secondary $^{13}C_{\alpha}$ and $^{13}C'$ chemical shifts. The helix stability is probably associated with formation of an N-capping hydrogen bond between the side-chain oxygen of D288 and the main-chain amide of E290 that is preferentially stabilized by P289 (22). The C-terminal region of Myb32, residues 302–310, also has a propensity for spontaneous helix formation, but to a much smaller extent (~20%).

c-Myb:KIX Interactions. Detailed examination of Myb32:KIX interactions by HSQC titrations and isothermal titration calorimetry (ITC) shows that KIX has two c-Myb binding sites. The ^{1}H-^{15}N HSQC spectrum of ^{15}N-labeled Myb32 bound to KIX at 1:1.2 mol ratio shows well-dispersed peaks (Fig. 1*B* and Fig. S1*A*, red peaks), indicating that c-Myb folds upon binding to KIX. However, on titration of substoichiometric concentrations of KIX into ^{15}N-labeled Myb32, several cross-peaks shift from their positions in the free Myb32 spectrum but do not move linearly to the positions for the fully bound Myb32:KIX complex (Fig. 1*B*). This shows that in addition to the primary, high-affinity site, c-Myb also binds to a secondary, lower-affinity site on KIX when in excess, as has been observed for pKID binding to KIX (10).

The location of the secondary c-Myb binding site can be determined by titration of ^{15}N-labeled KIX with unlabeled Myb32 (Fig. 1*D* and Fig. S1*B*). At substoichiometric concentrations of Myb32, the KIX HSQC peaks shift in slow exchange. Mapping of chemical shift perturbations at a 1:0.8 KIX:Myb32 ratio, referenced to free KIX, indicates that the primary c-Myb binding site on KIX overlaps with the pKID binding site (Fig. 2*A* and Fig. S1*C*), as shown in the structure of the Myb25:KIX complex (14). However, in the presence of excess Myb32, some KIX cross-peaks shift further in fast to intermediate exchange, indicating binding of c-Myb to a secondary site on KIX. The weighted average ^{15}N/^{1}H chemical shift changes at high Myb32 concentrations, referenced to the shifts at a 1:0.8 KIX:Myb32 ratio, are

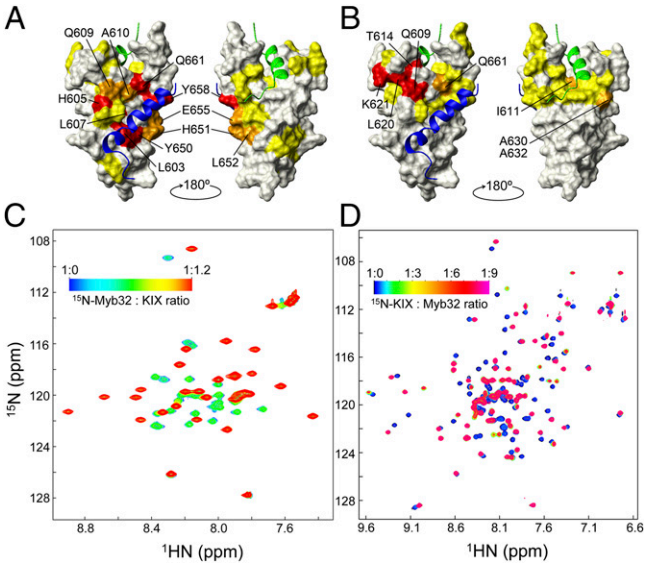

Fig. 2. c-Myb:KIX interactions. (*A* and *B*) Primary (*A*) and secondary (*B*) c-Myb binding sites on KIX. The weighted average chemical shift differences between the free and bound KIX amide resonances are mapped onto the surface of KIX in the KIX:c-Myb:MLL ternary complex (Protein Data Bank ID 2AGH) (14). Changes in chemical shift greater than 2 × SD from the mean (red), between 1 SD and 2 SD from the mean (orange), and between mean and 1 SD from the mean (yellow) are indicated. c-Myb (residues 290–315) and MLL (residues 2,842–2,860) are shown in blue and green, respectively. (*C*) ^{15}N-labeled Myb32 titration with KIX in the presence of a twofold excess of MLL28 over the KIX concentration. (*D*) ^{15}N-labeled KIX titration with Myb32 in the presence of MLL28 in a twofold excess to KIX. The cross-peak color changes gradually from blue (free) to red (bound) in *C* and from black (free) to magenta (bound) in *D* according to the concentration ratios shown.

large for residues Q609, I611, T614, L620, K621, A630, A632, and Q661 (Fig. 2*B* and Fig. S1*D*). These resonances are all sensitive to binding of peptides in the MLL site (12, 23), suggesting that the secondary c-Myb binding site on KIX overlaps with the MLL binding site.

The dissociation constants for the primary and secondary interactions of Myb32 with KIX, K_{d1} and K_{d2}, were estimated by ITC to be 0.23 ± 0.06 μM and 43 ± 14 μM, respectively (Fig. S2*A*). Global analysis of chemical shift changes (24) upon titration of ^{15}N-labeled KIX with Myb32, referenced to the shifts at a 1:0.8 KIX:Myb32 ratio, gives a K_{d2} of 46 ± 1 μM (Fig. S3*A*), in good agreement with the ITC results.

Suppression of Secondary c-Myb Binding to KIX. The presence of two c-Myb binding sites on KIX complicates analysis of the mechanism of coupled folding and binding. To simplify the binding process, we explored two strategies to eliminate the secondary c-Myb binding site. First we used the L628A mutant of KIX, which has a 100-fold lower affinity for MLL (23), to reduce the affinity of the secondary c-Myb binding site. However, on titration of KIX-L628A into ^{15}N-labeled Myb32, fast-exchange shifts of Myb32 were still observed at substoichiometric concentrations of KIX, showing the persistence of secondary c-Myb binding (Fig. S1*E*). In the second approach, excess MLL TAD (residues 2,842–2,869; MLL28) was added to the Myb32:KIX complex, to compete out the secondary c-Myb binding to the MLL site. This strategy worked well, and addition of twofold excess of MLL28 to KIX eliminated secondary c-Myb interactions in titrations of ^{15}N-labeled Myb32 with KIX and ^{15}N-labeled KIX with Myb32 (Fig. 2 *C* and *D*).

ITC experiments show that the K_d for Myb32 binding to the primary site on KIX in the presence of excess MLL28 is 0.213 ± 0.008 μM, which is similar to the K_{d1} measured in the absence of MLL28 (0.23 ± 0.06 μM) (Fig. S2*B*). These measurements indicate that Myb32 binds more tightly to KIX than does the shorter Myb25 construct (K_d = 10 ± 2 μM) (12).

Simulations of Myb32:KIX interactions over the range of concentrations used for R_2 relaxation dispersion experiments show that in the absence of MLL28, 91–96% of Myb32 binds to the primary c-Myb site on KIX, 3–9% binds to the secondary site, and 0.2–0.7% is in the free form (*SI Text* and Fig. S4 *A–C*). Because relaxation dispersion experiments are sensitive to low-abundance species (~1%), the presence of 3–9% of secondary c-Myb binding would complicate the study of the binding mechanism. On the other hand, simulations show that with MLL28 in twofold excess over KIX, 94–99% of Myb32 binds to the primary c-Myb site, 0.2–0.5% binds to the secondary c-Myb site, and 0.5–5.6% is in the free form (*SI Text* and Fig. S4 *D–G*). Under these conditions, relaxation dispersion experiments should be insensitive to binding in the secondary (MLL) site and will thus report only on c-Myb interactions with the primary binding site on KIX.

***R*$_2$ Relaxation Dispersion Analysis of c-Myb:KIX Binding.** The ^{15}N R_2 relaxation dispersion profiles for free Myb32 are completely flat, both in the presence and in the absence of MLL28 (Fig. S3*B*), indicating that any folding/unfolding transitions that occur in free Myb32 must be faster than ~10^5 s^{-1}. Indeed, helix-coil transitions generally occur in the nanosecond time range (at a rate of 10^7–10^8 s^{-1}) (25), very much faster than can be probed by R_2 relaxation dispersion. These NMR experiments also show that MLL28 does not interact with Myb32 and does not interfere with c-Myb folding or binding to KIX.

To monitor the binding of c-Myb to KIX, we performed ^{15}N R_2 relaxation dispersion experiments at two magnetic fields (^{1}H frequencies of 500 MHz and 800 MHz) for ^{15}N-labeled Myb32 bound to the KIX:MLL28 complex. Data were acquired over a range of Myb32:KIX:MLL28 concentration ratios (1:0.95:1.90, 1:1.00:2.00, 1:1.05:2.10, and 1:1.10:2.20), with MLL28 in a twofold excess over KIX. Acquisition of dispersion data at several concentration ratios is necessary to determine the c-Myb:KIX association rate. In total, eight dispersion curves were measured for each residue (Fig. 3*A*). In R_2 relaxation dispersion experiments, the effective transverse relaxation rate, R_2^{eff}, is the sum of the contribution from the exchange process, R_{ex}, and the intrinsic relaxation rate, R_2^0. Large R_{ex} values were observed for residues 290–292, 297–303, and 305–309 (Fig. 3*B* and Fig. S5), all of which are located in the helical region of KIX-bound c-Myb. The dispersion curves for each residue vary with changes in the Myb32:KIX concentration ratio, showing that the exchange arises from a binding event. Twelve residues exhibit well-defined dispersion curves (Fig. 3*A* and Fig. S6) and were used in the following analysis. The remaining c-Myb resonances exhibited weak or noisy dispersion curves, with small values of R_{ex} (Fig. 3*B*), or could not be analyzed because of cross-peak overlap.

The relaxation dispersion data were fitted using three different binding models (Fig. 4). Model 1 is a two-site exchange model, which assumes that free c-Myb folds and binds to KIX without formation of observable intermediates. The other models invoke formation of an intermediate, i.e., are three-site exchange models. Model 2 assumes that c-Myb first binds to KIX to form an intermediate and that folding is completed on the surface of KIX (5). In model 3, binding proceeds via a process of conformational selection, in which KIX binds selectively to a preferred conformer within the c-Myb conformational ensemble. If the rate of folding of free c-Myb to form the binding-competent conformation (k_{UH}) is slower than the rate of association with KIX (k_{ON} [KIX]) and slow enough to be detectable by R_2 relaxation dispersion, then binding would be modeled by a three-state process (model 3a). However, if the folding and unfolding processes of free c-Myb are very fast and are invisible on the relaxation dispersion timescale, then the conformational selection model reduces to an apparent two-site exchange mechanism (model 3b). For this mechanism, the association rate would be directly proportional to the population of correctly folded (helical) states in the conformational ensemble of the free c-Myb peptide.

The dispersion curves for 12 residues at four concentration ratios and at two magnetic fields (a total of 96 curves) were fitted globally, using each of these models to obtain accurate estimates of rates and chemical shift differences (details in *SI Text* and Table S1). Fits to models 2 and 3a resulted in parameters that are physically unreasonable (details in Fig. S7). In addition, the fitted c-Myb conformational exchange rates (k_{UH} = 1,900 s^{-1}, k_{HU} = 12,000 s^{-1}) are 10^3–10^4 times slower than expected for helix-coil transitions in peptides (25) and are not consistent with the flat R_2 dispersion profiles observed for free c-Myb (Fig. S3*B*). By contrast, the fit to the two-state model, where the association rate (k_{ON}), the dissociation rate (k_{OFF}), and the chemical shift

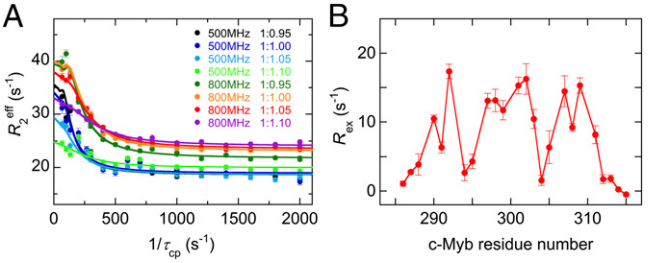

Fig. 3. R_2 relaxation dispersion experiments. (*A*) ^{15}N R_2 relaxation dispersion profile for L301 of Myb32 recorded at 500-MHz and 800-MHz spectrometers and at 1:0.95–1:1.10 Myb32:KIX concentration ratios in the presence a twofold excess of MLL28 over KIX. (*B*) ^{15}N R_{ex} of Myb32 at 500 MHz at a concentration ratio of 1:0.95:1.90 Myb32:KIX:MLL28. R_{ex} was estimated from the differences in R_2^{eff} at the lowest and highest $1/\tau_{cp}$ values. Errors were estimated from duplicate measurements (10).

Model 1: two-state model

$$\text{c-Myb + KIX}\ (\text{free}) \underset{k_{OFF}}{\overset{k_{ON}[KIX]}{\rightleftharpoons}} \text{c-Myb:KIX}\ (\text{bound})$$

Model 2: induced-fit model

$$\text{c-Myb + KIX}\ (\text{free (F)}) \underset{k_{OFF}}{\overset{k_{ON}[KIX]}{\rightleftharpoons}} \text{c-Myb*:KIX}\ (\text{intermediate (I)}) \underset{k_{BI}}{\overset{k_{IB}}{\rightleftharpoons}} \text{c-Myb:KIX}\ (\text{bound (B)})$$

Model 3a: conformational selection model

$$\text{c-Myb}^{U}\ (\text{unfolded (U)}) \underset{k_{HU}}{\overset{k_{UH}}{\rightleftharpoons}} \text{c-Myb}^{H}\ (\text{helical (H)}) + \text{KIX} \underset{k_{OFF}}{\overset{k_{ON}[KIX]}{\rightleftharpoons}} \text{c-Myb:KIX}\ (\text{bound (B)})$$

Model 3b: conformational selection model with fast pre-equilibrium

$$\underbrace{\left[\text{c-Myb}^{U} \underset{k_{HU}}{\overset{k_{UH}}{\rightleftharpoons}} \text{c-Myb}^{H}\right]}_{\text{fast pre-equilibrium}} + \text{KIX} \underset{k_{OFF}}{\overset{k_{ON}[KIX]}{\rightleftharpoons}} \text{c-Myb:KIX}\ (\text{bound (B)})$$

Fig. 4. Representative mechanisms of coupled folding and binding reactions of IDPs. k_{ON} and k_{OFF} are the association and dissociation rates for c-Myb binding to KIX; k_{IB} and k_{BI} are the rates for the folding and unfolding reactions of c-Myb on the surface of KIX; k_{UH} and k_{HU} are the folding and unfolding rates of free c-Myb; c-Myb* denotes c-Myb in disordered structures; and c-Myb^{U} and c-Myb^{H} denote free c-Myb in the unfolded and helical states, respectively.

difference are fitted independently for each residue, gives physically reasonable parameters. The average k_{ON} and k_{OFF} values are $(1.7 \pm 0.1) \times 10^{7}$ $M^{-1}{\cdot}s^{-1}$ and 14.6 ± 0.7 s^{-1}, respectively (Fig. 5 *A* and *B*). The small k_{OFF} value is consistent with the slow-exchange behavior observed in the ^{15}N-Myb32 titration with KIX for the primary c-Myb binding process. ^{15}N chemical shift differences between the free and bound forms ($\Delta\omega_{FB}$) obtained from the fits to the R_2 relaxation dispersion data are strongly correlated with equilibrium shift differences obtained by HSQC titrations ($\Delta\delta_{FB}$), indicating that the weakly populated state detected by the R_2 relaxation dispersion experiments is the free form of Myb32 (Fig. 5*C*). Nevertheless, the mechanism of c-Myb binding is more complicated than a simple two-state process. Whereas the k_{ON} values remain similar throughout the sequence, the k_{OFF} values differ significantly between the N- and C-terminal portions of c-Myb.

Discussion

Upon binding to KIX or to the KIX:MLL complex, residues 293–309 of the intrinsically disordered c-Myb activation domain fold to form a long amphipathic helix with a distinct bend at M303/S304 that enables the side chain of L302 to penetrate deeply into a hydrophobic pocket in the surface of KIX (13, 14). The bend in the bound c-Myb helix forms two helical segments, K293–L301/L302, and L302/M303–L309. Both segments of c-Myb make extensive hydrophobic and electrostatic contacts with KIX (13).

Mechanism of Coupled Folding and Binding of c-Myb. By adding MLL to suppress secondary c-Myb binding to KIX, we were able to study the mechanism of direct binding of c-Myb to the primary, high-affinity site on KIX without any of the modifications that were introduced in previous stopped-flow kinetics studies (26–28). The ^{15}N R_2 relaxation dispersion experiments clearly show that c-Myb binds to KIX by an apparent two-state mechanism, without formation of observable intermediates. Attempts to fit the data to an induced-fit mechanism (model 2) or the slow conformational selection mechanism of model 3a were unsuccessful (Fig. S7).

Because free Myb32 is dynamically disordered, averaging over an ensemble of conformations that includes both helical and more extended states, the effective association and dissociation rates at each residue could vary slightly. The apparent variations in the fitted k_{ON} values in Fig. 5*A* are not statistically significant; the relaxation dispersion data could be fitted well when k_{ON} was constrained globally or constrained separately for clusters of residues in the N- and C-terminal segments of the bound c-Myb helix (details in *SI Text*). We thus conclude that, within our experimental uncertainties, the association rate is the same for all residues. This is not the case, however, for the dissociation rate. Attempts to fit the relaxation dispersion data with a global k_{OFF} value for all residues resulted in a notably poorer fit than that obtained from individual fits (*SI Text* and Table S1), and it is clear that the effective dissociation rate of residues 302–309 is slightly slower (average 12.7 s^{-1}) than for those in the N-terminal segment of the bent c-Myb helix (average k_{OFF} 16.6 s^{-1}). The fact that the relaxation dispersion data cannot be fitted well using a global k_{OFF} suggests that dissociation may not occur via a global process, in which the entire c-Myb domain dissociates from the surface of KIX in a single step. Rather, dissociation appears to occur by a localized unfolding mechanism, in which local regions of the bent helix unfold and undock at slightly different rates.

In the unbound state, the N- and C-terminal parts of the bent c-Myb helix exhibit different conformational propensities (Fig. 1*C*). Residues 290–301 have a strong propensity to fold spontaneously into a helical structure, which is 70% populated in free Myb32. In contrast, residues 302–310 have a much smaller propensity to fold in the absence of KIX, with only 20% population of helix in the unbound state. Given the very high population of helix between residues 290 and 301 in the conformational ensemble of free Myb32, it is probable that this region of the peptide docks to KIX predominantly in a folded or partially folded state. Although the population of helix in the N-terminal region of free Myb25 is smaller (~20% for residues 291–301), substitution of glycine (but not alanine) for E297 or L300, which is predicted by AGADIR (22) to greatly decrease the population

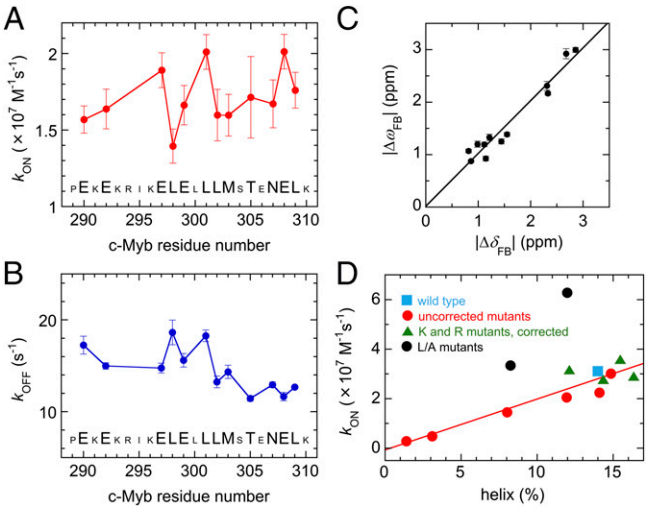

Fig. 5. Kinetic and structural parameters derived from relaxation dispersion experiments. (*A* and *B*) k_{ON} (*A*) and k_{OFF} (*B*) for c-Myb residues, obtained by fitting to the two-state model. Large characters indicate the 12 residues used in global analysis of the dispersion curves. Error bars show fitting errors. (*C*) Correlation of ^{15}N chemical shift differences ($\Delta\omega_{FB}$) for Myb32 determined by fitting the dispersion curves to the two-state model with equilibrium ^{15}N chemical shift differences ($\Delta\delta_{FB}$) between free Myb32 and the KIX-bound form in the presence of MLL28. The linear regression line (slope = 1.01, *y* intercept = 0.02, correlation coefficient r = 0.97) is shown. (*D*) Correlation between the association rate for binding of c-Myb mutants to KIX [data taken from Giri et al. (27)] and the intrinsic population of helix between residues 293 and 303 in the mutant Myb25 peptides predicted by AGADIR (22). Full details are given in *SI Text*.

of helix in free Myb25 without interfering with c-Myb–KIX contacts in the bound state, results in an ∼10-fold decrease in k_{ON} and a large increase in k_{OFF} (27). In contrast, helix-destabilizing glycine substitutions in the C-terminal part of the c-Myb helix have little effect on the Myb25 association rate. Because the binding process is two-state, the NMR dispersion experiments can provide no insights into whether the C-terminal segment of the bent c-Myb helix, which is less structured in free Myb32, folds before or after binding to KIX.

Recent stopped-flow kinetics data are consistent with our NMR relaxation dispersion experiments in showing that binding of c-Myb to KIX occurs by a two-state process, without observable intermediates (26, 28). Binding is extremely fast and appears to exceed the association rate expected for globular proteins of this size (28). Giri et al. (27) have recently applied site-directed mutagenesis (Φ-value analysis) to probe the structure of the transition state for binding of Myb25 to the Y658W mutant of KIX. The transition state possesses a high degree of native-like secondary and tertiary structure, with folding nuclei located in the N- and C-terminal regions of the bent helix.

Based on the observation that the Myb25:KIX association rate is not affected by addition of 5–7% trifluoroethanol, which promotes partial stabilization of helix, and on the basis of an extrapolation of association rates for long and short forms of fluorescently labeled c-Myb, with differing populations of helix, to infinite ionic strength, Gianni et al. (26) and Shammas et al. (29) concluded that the association rate is not correlated with the helical content of free c-Myb and that folding is induced by binding to the surface of KIX. Our relaxation dispersion data suggest that the actual binding and folding mechanism is likely to be more complex. The 70% population of helix in the N-terminal region of free Myb32 implies that the helix will be preformed in a high proportion of c-Myb:KIX encounters, i.e., that folding occurs before binding. In contrast, the C-terminal region of free Myb32 exhibits a much smaller helical propensity (∼20%) and it is likely that folding, which takes place before formation of the transition state (27), occurs after binding to KIX.

Given the high probability that the initial encounter events would involve interactions with helical states of c-Myb, we decided to reexamine the mechanism of c-Myb binding to KIX, using the extensive mutagenesis data of Giri et al. (27) and predictions of the intrinsic helical propensities in the N-terminal region of the various c-Myb mutants. We found a direct (1:1) correlation between the population of helix between residues 293 and 303, predicted by the program AGADIR (22) for the wild-type and mutant Myb25 peptides, and the association rates measured by Giri et al. (27) for binding of Myb25 to KIX (Fig. 5*D*); an *n*-fold change in the population of helix corresponds to the same *n*-fold change in k_{ON}. A direct correlation between the association rate and the population of helix in the conformational ensemble of unbound c-Myb is fully consistent with the conformational selection mechanism of our model 3b, in which there is very fast exchange between folded and unfolded states of free c-Myb. The fact that the association rate increases linearly with increasing population of helix in the N-terminal region of c-Myb provides direct evidence that the initial binding event involves folded helical conformers within the free c-Myb conformational ensemble. It is important to note that this conformational selection process involves only the N-terminal region of c-Myb; helix-breaking Gly mutations in the C-terminal region of c-Myb result in an increase in association rates and a change in folding pathways (as indicated by Φ values greater than unity) (27), suggesting an induced-fit folding mechanism for this region.

Comparison with pKID. The present results clearly show that two different IDPs, pKID and c-Myb, can bind the same site of KIX by different binding mechanisms. pKID binds KIX by an induced-fit mechanism, forming a partly folded intermediate that becomes stabilized by intermolecular interactions formed in the final bound state (10). By contrast, c-Myb binds KIX by an apparent two-state mechanism, in which folding occurs simultaneously with or before binding.

Because the association rates for c-Myb (1.7×10^7 $M^{-1}{\cdot}s^{-1}$) and pKID (on average, 6.3×10^6 $M^{-1}{\cdot}s^{-1}$) (10) are similar, it is likely that differences in the folding rates of c-Myb and pKID play a role in determining the binding mechanism. From the present study, the association time constant for Myb32 is ∼80 μs [$= 1/(1.7 \times 10^7\ M^{-1}{\cdot}s^{-1} \times 0.7\ mM)$], indicating that the timescale for c-Myb folding is faster than 80 μs. This is consistent with laser temperature jump studies of helical peptides, which show that formation of helix can occur on a 100-ns timescale (25). Thus, the Myb32 peptide can rapidly sample native-like helical states on a timescale that is much faster than the actual binding event. In contrast to c-Myb, the C-terminal (αB) helix of KIX-bound pKID, which makes the dominant contribution to the free energy of binding (8), has very low intrinsic propensity to form helix and is largely unstructured in the free KID or pKID peptides (Fig. S8) (9). The αB helix remains only partly folded in the pKID:KIX binding intermediate and folds into the helical structure of the fully bound state at a rate that is slow compared with the rate of association of pKID with KIX (10). In contrast, the αA helix of pKID, which spontaneously forms ∼50% population of helix in the free peptide (9), is fully folded in the pKID:KIX intermediate. It appears that differences in the helical propensities of pKID and c-Myb may be primary determinants of the folding rate and thus the binding mechanism. We suggest that the very weak helical propensity of the αB region of pKID may present a barrier to folding and that formation and stabilization of helical structure in this region may require establishment of favorable intermolecular interactions after docking to the surface of KIX.

The differing propensities for spontaneous helix formation by pKID and c-Myb appear to be closely related to their functions. CREB is an inducible transcriptional activator that requires phosphorylation of S133 in the KID domain for high-affinity binding to KIX. The high degree of disorder and low propensity for secondary structure formation in the αB region and in the vicinity of S133 of KID are expected to facilitate interaction with and phosphorylation by protein kinase A (8), which binds peptide substrates in a relatively extended conformation (30). On the other hand, c-Myb is a constitutive transcriptional activator, which does not require post-translational modification for high-affinity binding to KIX, and its strong propensity for helix formation may be advantageous for rapid activation of Myb-mediated transcriptional programs. There is growing evidence that the intrinsic helical propensity of an IDP is finely tuned by the sequence and is an important determinant of both its biological function and its binding affinity and mechanism. This has been recently demonstrated most elegantly for the disordered activation domain of p53, where mutations that increase the population of preformed helical structure alter the dynamics of p53 accumulation and impair the p53 response to DNA damage (31). Likewise, mutations that decrease the helical propensity of a linker region in the p27 cyclin-dependent kinase inhibitor impair its ability to promote cell cycle arrest (32).

Because IDPs vary greatly in their conformational propensities, it is not surprising that they do not use a common mechanism for binding and folding and that both conformational selection and induced-fit mechanisms, or a combination of both, have been observed for binding of various IDPs to their targets. The transition state for binding of c-Myb to KIX differs from those of other IDPs that have been studied to date in that Φ values and linear free energy relationships show that near-native secondary and tertiary structure has already formed at the top of the rate-limiting energy barrier (27). In contrast, the transition states for binding and folding of S peptide to S protein (33), the IDP PUMA to its MCL-1 target (34), and the activation domain of ACTR to the nuclear coactivator binding domain (NCBD) of CBP (35) are located early in the binding pathway; folding of the IDP and formation of native intermolecular interactions occur after the rate-limiting step for

binding, i.e., by an induced-fit mechanism. Whereas native-like ACTR–NCBD interactions are mostly formed late in the reaction pathway, mutations that increase the propensity for spontaneous helix formation in the N-terminal region of ACTR accelerate binding by a conformational selection mechanism (36). Thus, the ACTR–NCBD interaction is complex: Different regions of the intrinsically disordered ACTR bind and fold by different pathways, consistent with computer simulations (37). It seems likely that the involvement of both conformational selection and induced fit will emerge as a common framework for binding and folding processes of all but the simplest IDPs.

NMR relaxation dispersion experiments provide atomic resolution insights into IDP binding and folding mechanisms that complement conventional kinetics measurements. Whereas binding and folding of c-Myb occur by a two-state process (this work), dispersion experiments show that both pKID and the disordered NTAIL domain from Sendai virus nucleoprotein associate with their target proteins (KIX and the phosphoprotein PX, respectively) by three-state mechanisms involving formation of an intermediate (10, 18). Whereas NTAIL binds rapidly to PX to form a dynamic encounter complex, with a preformed helical state of free NTAIL docked to PX, native intermolecular interactions develop more slowly at a rate that is determined by motions of a helical groove on the surface of PX itself (18).

In conclusion, the available kinetics and NMR data show clearly that coupled folding and binding reactions of IDPs do not obey a single, general mechanism. Rather, binding occurs by a variety of mechanisms, depending on the conformational propensities of the IDPs themselves, as well as the intrinsic conformational dynamics of their target proteins (18).

Materials and Methods

Protein Expression and Purification. Details for the preparation of Myb32 are given in *SI Text*. Myb25, MLL28, and the KIX domain (residues 586–672) of mouse CBP were prepared as described previously (6, 8, 13, 14, 23).

CD, ITC, and NMR Measurements. Full details of the CD, ITC, and NMR measurements are given in *SI Text*. ^{15}N R_2 relaxation dispersion data were acquired at 30 °C, using relaxation-compensated constant-time Carr–Purcell–Meiboom–Gill (CPMG) pulse sequences (10, 38) with a constant relaxation delay of 40 ms or 60 ms.

ACKNOWLEDGMENTS. We thank Maria Martinez-Yamout for assistance with sample preparation and Gerard Kroon for NMR measurements. This work was supported by Grant CA096865 from the National Institutes of Health and by the Skaggs Institute for Chemical Biology. M.A. was supported by Grants-in-Aid for Scientific Research from the Ministry of Education, Culture, Sports, Science, and Technology of Japan; by the Kurata Memorial Hitachi Science and Technology Foundation; by the Sumitomo Foundation; by the Asahi Glass Foundation; and by Precursory Research for Embryonic Science and Technology, Japan Science and Technology Agency.

1. Wright PE, Dyson HJ (1999) Intrinsically unstructured proteins: Re-assessing the protein structure-function paradigm. *J Mol Biol* 293(2):321–331.
2. Dunker AK, et al. (2001) Intrinsically disordered protein. *J Mol Graph Model* 19(1):26–59.
3. Uversky VN (2002) Natively unfolded proteins: A point where biology waits for physics. *Protein Sci* 11(4):739–756.
4. Dyson HJ, Wright PE (2005) Intrinsically unstructured proteins and their functions. *Nat Rev Mol Cell Biol* 6(3):197–208.
5. Wright PE, Dyson HJ (2009) Linking folding and binding. *Curr Opin Struct Biol* 19(1):31–38.
6. Radhakrishnan I, et al. (1997) Solution structure of the KIX domain of CBP bound to the transactivation domain of CREB: A model for activator:coactivator interactions. *Cell* 91(6):741–752.
7. Parker D, et al. (1996) Phosphorylation of CREB at Ser-133 induces complex formation with CREB-binding protein via a direct mechanism. *Mol Cell Biol* 16(2):694–703.
8. Zor T, Mayr BM, Dyson HJ, Montminy MR, Wright PE (2002) Roles of phosphorylation and helix propensity in the binding of the KIX domain of CREB-binding protein by constitutive (c-Myb) and inducible (CREB) activators. *J Biol Chem* 277(44):42241–42248.
9. Radhakrishnan I, Pérez-Alvarado GC, Dyson HJ, Wright PE (1998) Conformational preferences in the Ser^{133}-phosphorylated and non-phosphorylated forms of the kinase inducible transactivation domain of CREB. *FEBS Lett* 430(3):317–322.
10. Sugase K, Dyson HJ, Wright PE (2007) Mechanism of coupled folding and binding of an intrinsically disordered protein. *Nature* 447(7147):1021–1025.
11. Goodman RH, Smolik S (2000) CBP/p300 in cell growth, transformation, and development. *Genes Dev* 14(13):1553–1577.
12. Goto NK, Zor T, Martinez-Yamout M, Dyson HJ, Wright PE (2002) Cooperativity in transcription factor binding to the coactivator CREB-binding protein (CBP). The mixed lineage leukemia protein (MLL) activation domain binds to an allosteric site on the KIX domain. *J Biol Chem* 277(45):43168–43174.
13. Zor T, De Guzman RN, Dyson HJ, Wright PE (2004) Solution structure of the KIX domain of CBP bound to the transactivation domain of c-Myb. *J Mol Biol* 337(3):521–534.
14. De Guzman RN, Goto NK, Dyson HJ, Wright PE (2006) Structural basis for cooperative transcription factor binding to the CBP coactivator. *J Mol Biol* 355(5):1005–1013.
15. Oh IH, Reddy EP (1999) The myb gene family in cell growth, differentiation and apoptosis. *Oncogene* 18(19):3017–3033.
16. Parker D, et al. (1999) Role of secondary structure in discrimination between constitutive and inducible activators. *Mol Cell Biol* 19(8):5601–5607.
17. Palmer AG, 3rd, Kroenke CD, Loria JP (2001) Nuclear magnetic resonance methods for quantifying microsecond-to-millisecond motions in biological macromolecules. *Methods Enzymol* 339:204–238.
18. Schneider R, et al. (2015) Visualizing the molecular recognition trajectory of an intrinsically disordered protein using multinuclear relaxation dispersion NMR. *J Am Chem Soc* 137(3):1220–1229.
19. Schwarzinger S, et al. (2001) Sequence-dependent correction of random coil NMR chemical shifts. *J Am Chem Soc* 123(13):2970–2978.
20. Tamiola K, Acar B, Mulder FAA (2010) Sequence-specific random coil chemical shifts of intrinsically disordered proteins. *J Am Chem Soc* 132(51):18000–18003.
21. Yao J, Chung J, Eliezer D, Wright PE, Dyson HJ (2001) NMR structural and dynamic characterization of the acid-unfolded state of apomyoglobin provides insights into the early events in protein folding. *Biochemistry* 40(12):3561–3571.
22. Muñoz V, Serrano L (1994) Elucidating the folding problem of helical peptides using empirical parameters. *Nat Struct Biol* 1(6):399–409.
23. Arai M, Dyson HJ, Wright PE (2010) Leu628 of the KIX domain of CBP is a key residue for the interaction with the MLL transactivation domain. *FEBS Lett* 584(22):4500–4504.
24. Arai M, Ferreon JC, Wright PE (2012) Quantitative analysis of multisite protein-ligand interactions by NMR: Binding of intrinsically disordered p53 transactivation subdomains with the TAZ2 domain of CBP. *J Am Chem Soc* 134(8):3792–3803.
25. Ferguson N, Fersht AR (2003) Early events in protein folding. *Curr Opin Struct Biol* 13(1):75–81.
26. Gianni S, Morrone A, Giri R, Brunori M (2012) A folding-after-binding mechanism describes the recognition between the transactivation domain of c-Myb and the KIX domain of the CREB-binding protein. *Biochem Biophys Res Commun* 428(2):205–209.
27. Giri R, Morrone A, Toto A, Brunori M, Gianni S (2013) Structure of the transition state for the binding of c-Myb and KIX highlights an unexpected order for a disordered system. *Proc Natl Acad Sci USA* 110(37):14942–14947.
28. Shammas SL, Travis AJ, Clarke J (2013) Remarkably fast coupled folding and binding of the intrinsically disordered transactivation domain of cMyb to CBP KIX. *J Phys Chem B* 117(42):13346–13356.
29. Shammas SL, Travis AJ, Clarke J (2014) Allostery within a transcription coactivator is predominantly mediated through dissociation rate constants. *Proc Natl Acad Sci USA* 111(33):12055–12060.
30. Taylor SS, et al. (2005) Dynamics of signaling by PKA. *Biochim Biophys Acta* 1754(1–2):25–37.
31. Borcherds W, et al. (2014) Disorder and residual helicity alter p53-Mdm2 binding affinity and signaling in cells. *Nat Chem Biol* 10(12):1000–1002.
32. Otieno S, Kriwacki R (2012) Probing the role of nascent helicity in p27 function as a cell cycle regulator. *PLoS One* 7(10):e47177.
33. Bachmann A, Wildemann D, Praetorius F, Fischer G, Kiefhaber T (2011) Mapping backbone and side-chain interactions in the transition state of a coupled protein folding and binding reaction. *Proc Natl Acad Sci USA* 108(10):3952–3957.
34. Rogers JM, et al. (2014) Interplay between partner and ligand facilitates the folding and binding of an intrinsically disordered protein. *Proc Natl Acad Sci USA* 111(43):15420–15425.
35. Dogan J, Mu X, Engström Å, Jemth P (2013) The transition state structure for coupled binding and folding of disordered protein domains. *Sci Rep* 3:2076.
36. Iešmantavičius V, Dogan J, Jemth P, Teilum K, Kjaergaard M (2014) Helical propensity in an intrinsically disordered protein accelerates ligand binding. *Angew Chem Int Ed Engl* 53(6):1548–1551.
37. Zhang W, Ganguly D, Chen J (2012) Residual structures, conformational fluctuations, and electrostatic interactions in the synergistic folding of two intrinsically disordered proteins. *PLoS Comput Biol* 8(1):e1002353.
38. Loria JP, Rance M, Palmer AG, III (1999) A relaxation-compensated Carr-Purcell-Meiboom-Gill sequence for characterizing chemical exchange by NMR spectroscopy. *J Am Chem Soc* 121:2331–2332.
39. Delaglio F, et al. (1995) NMRPipe: A multidimensional spectral processing system based on UNIX pipes. *J Biomol NMR* 6(3):277–293.
40. Johnson BA, Blevins RA (1994) NMR View: A computer program for the visualization and analysis of NMR data. *J Biomol NMR* 4(5):603–614.
41. Wang ZX, Jiang RF (1996) A novel two-site binding equation presented in terms of the total ligand concentration. *FEBS Lett* 392(3):245–249.
42. Press WH, Flannery BP, Teukolsky SA, Vetterling WT (1992) *Numerical Recipes in Fortran 77. The Art of Scientific Computing* (Cambridge Univ Press, Cambridge, UK).
43. Sugase K, Konuma T, Lansing JC, Wright PE (2013) Fast and accurate fitting of relaxation dispersion data using the flexible software package GLOVE. *J Biomol NMR* 56(3):275–283.
44. Carver JP, Richards RE (1972) A general two-site solution for chemical exchange produced dependence of T_2 upon Carr-Purcell pulse separation. *J Magn Reson* 6(1):89–105.